

Batch-to-batch model improvement for cooling crystallization

Marco Forgione^{a,*}, Georgios Birpoutsoukis^e, Xavier Bombois^a, Ali Mesbah^b,
Peter J. Daudey^c, Paul M.J. Van den Hof^d

^a*Laboratoire Ampère UMR CNRS 5005, Ecole Centrale de Lyon, Ecully, France*

^b*Department of Chemical and Biomolecular Engineering, University of California, Berkeley, USA*

^c*Chemical Engineering Department, Delft University of Technology, The Netherlands*

^d*Department of Electrical Engineering, Eindhoven University of Technology, Eindhoven, The Netherlands*

^e*Vrije Universiteit Brussel, Department ELEC, Brussel, Belgium*

Abstract

Two batch-to-batch model update strategies for model-based control of batch cooling crystallization are presented. In Iterative Learning Control, a nominal process model is adjusted by a non-parametric, additive correction term which depends on the difference between the measured output and the model prediction in the previous batch. In Iterative Identification Control, the uncertain model parameters are iteratively estimated using the measured batch data. Due to the different nature of the model update, the two algorithms have complementary advantages and disadvantages which are investigated in a simulation study and through experiments performed on a pilot-scale crystallizer. ¹

Keywords: System identification, Iterative learning control, Process control, Batch processes, Batch cooling crystallization.

*Corresponding author

Email address: marco.forgione@ec-lyon.fr (Marco Forgione)

¹The financial support of the Institute for Sustainable Process Technology (ISPT) under the grant ISPT PH-00-04 is gratefully acknowledged.

1. Introduction

Cooling crystallization is a separation and purification process often performed in batch mode in the pharmaceutical, food and fine chemicals industries for the production of high value-added products [14]. In a batch cooling crystallization process, a solution consisting of a solute dissolved in a solvent is loaded at high temperature into a vessel called crystallizer, and is subsequently cooled down. The crystallizer temperature is manipulated by circulating a cooling medium inside the jackets surrounding the crystallizer. Due to cooling, the equilibrium concentration of the solution (i.e. the solubility) is lowered and part of the solute is transferred from the solution to the solid crystalline phase. The content of the crystallizer is no longer a clear solution, but a two-phase fluid slurry consisting of the solution and the solid crystals. The concentration of the solute in the solution decreases, while the amount of solid crystals increases. When the final temperature corresponding to the desired yield is reached, the solid crystals are separated from the solution and the batch ends.

In industrial batch cooling crystallizers, the crystallizer temperature is often the only process variable that is controlled [6]. The jacket temperature is the manipulated variable used to steer the crystallizer temperature. Since accurate on-line temperature measurements can be readily obtained, the crystallizer temperature is controlled in a closed-loop setting. In this configuration, the desired cooling profile is given as set-point to a feedback temperature control loop.

However, even when the temperature is effectively controlled, the crystal product of a batch might not show all the desired properties. In fact, even though the temperature is an important process variable, it is not the one most closely related to the crystallization dynamics. The process variable having the most direct influence on the crystallization process is the supersaturation, often defined as the difference between the solute concentration and the solubility at a given temperature. Supersaturation is the driving force for physico-chemical phenomena involved in crystallization such as the birth and the growth of crystals [14], and its trajectory throughout the process influences several aspects of the final product including chemical purity, polymorphic state, crystal size and shape [18, 1]. In general, operating at too high supersaturation has to be avoided since it leads to a degradation of the product quality. Conversely, operating at low supersaturation leads to a slow growth of the crystals and therefore to a low production rate. A

trade-off between product quality and productivity is often defined by aiming at a constant supersaturation during the batch time [12, 6, 7].

In a batch cooling crystallization process, the supersaturation can be manipulated by changing the crystallizer temperature, since the latter determines the solubility. Supersaturation control strategies for batch cooling crystallization have been widely investigated in the literature [15, 23, 21, 6]. In general, supersaturation control has been shown to give better performance compared to temperature control only, particularly in terms of consistency of the product quality.

In most of the supersaturation control strategies, a nominal model of the supersaturation dynamics is used to design the model-based controller. Therefore, the quality of the model has a direct influence on the tracking performance that the model-based controller can achieve. Unfortunately, the models describing the process often suffer from severe uncertainties. Due to these uncertainties, the performance delivered by the model-based controller can significantly deteriorate in the case of a model-plant mismatch.

This paper investigates the opportunity of using input/output data collected from previous batches in order to improve the model, and consequently the performance delivered by a model-based control solution. In particular a situation is considered in which the concentration measurements collected throughout a batch (which are required in order to compute the supersaturation) are available for control only at the end of the batch. This situation can occur in an industrial environment, where the measurements are often obtained through the off-line analysis of samples collected throughout the batch. The quality of the model is even more important than in the case of feedback control. Indeed, feedforward control solutions are in general more sensitive to model-plant mismatches than the ones based on on-line feedback.

In [5, 4], the authors introduced a novel batch-to-batch (B2B) control strategy conceived in order to track efficiently a supersaturation profile in a batch cooling crystallization process, under the presence of disturbances and model uncertainties. The findings presented in those previous contributions, which were obtained using a simulation model of the process, are here complemented with the results of real experiments performed on a pilot-scale crystallization setup which confirm the applicability of our method. To the best of the authors' knowledge, these are the first B2B control experiment for a batch cooling crystallization process documented in the literature.

The B2B control strategy exploits the fact that the concentration measurements are only available off-line, but the temperature measurements are

readily available on-line. In fact, an higher-level B2B supersaturation control algorithm is combined with a lower-level feedback PI temperature controller. Based on the desired supersaturation profile and the off-line concentration measurements from the previous batches, the B2B algorithm updates a model of the process dynamics. Subsequently, it uses the updated model in order to compute an improved reference temperature profile T^r . This profile is set as reference to a lower-level PI temperature controller in the next batch. The role of the PI controller is to suppress the system disturbances as efficiently as possible in order to decrease their influence on the supersaturation dynamics.

Two B2B algorithms, namely Iterative Identification Control (IIC) and Iterative Learning Control (ILC) are presented. While IIC is based on a parametric model update, ILC performs a more flexible, nonparametric model correction. Due to the different nature of the model update, the two algorithms have complementary advantages and disadvantages, which are investigated in this paper.

The ILC algorithm used in this paper is based on the two-step procedure first introduced in [22]. After a batch, the model of the dynamics from the reference temperature T^r to the supersaturation S is updated using a non-parametric additive correction term, which depends on the difference between the measured supersaturation and the supersaturation predicted by the model for the previous batch. This correction term is obtained in such a way that the updated model matches more closely the actual supersaturation measured during the previous batch. Subsequently, the improved reference temperature is computed using the updated model in order to minimize the supersaturation tracking error for the next batch. In the literature, other applications of ILC for supersaturation control in batch cooling crystallization have been presented in [24, 18]. In both algorithms, a new temperature trajectory is designed based on a linear time-varying perturbation model of the nonlinear supersaturation dynamics. Compared to those papers, the advantage of the approach presented here is twofold. First, the presence of a lower-level PI controller, which is an asset in the presence of disturbances on the temperature dynamics. The ILC algorithm alone, which is a feedforward control solution, could not compensate for these real-time disturbances. In addition, these disturbances could be easily confused by the algorithm with parts of the actual process dynamics since ILC is based on a non-parametric model correction. Second, the use of the nonlinear, first-principles model of the process in the algorithm, as opposed to the linearized model used in

[24, 18], which is an acceptable approximation of the dynamics only along the time-varying working point. Besides, it has to be mentioned that while in [24, 18] only simulation results have been reported, in this paper experimental results are also included.

In the IIC algorithm, estimates of the uncertain physical parameters are refined after a batch according to a Maximum a Posteriori criterion which combines the information coming from the measurements collected during the most recent batch with the previous parameter estimates. By doing this, the accuracy of the model increases after each batch, since the parameter estimates are obtained using an increasing amount of information. Next, as in the ILC algorithm, the reference temperature T^r for the next batch is optimized off-line using the updated model in order to follow the desired supersaturation set-point.

The remainder of the paper is organized as follows. First, a model for the batch cooling crystallization process is presented in Section 2. Subsequently, the B2B control framework is discussed in Section 3. The framework is applied in a simulation study in Section 4 and on the pilot-scale crystallizer in Section 5. Finally, overall conclusions and directions for future research are discussed in Section 6.

2. The batch cooling crystallization model

A model of the batch cooling crystallization process is presented in this Section. This model is used extensively throughout this paper. First, it is used in Section 3 for the design of the B2B control algorithms. Second, the data-generating system used in Section 4 to represent the crystallizer in the simulation study is a numerical implementation on this model. Finally, the B2B control algorithms based on this model are applied on the real pilot-scale crystallization setup in Section 5.

As previously discussed in the introduction, in a batch cooling crystallization process a chemical solution is cooled down in a crystallizer. The jacket temperature T_J is the manipulated variable used to steer the crystallizer temperature T .² By cooling, the solubility of the solution is lowered,

²In practice, the jacket temperature T_J is not directly manipulated, but it is controlled by a low-level control loop. The set-point of the low-level controller is the variable that is actually accessible (See the description of experimental set-up in Section 5.1). However, the dynamics of this low-level control loop is usually much faster compared to the other

and part of the solute is transferred from the solution to the solid, crystalline phase. Therefore, the concentration C of the solute within the solution decreases. The batch cooling crystallization process is often represented using the so-called *moment model* [16]. A state-space representation of this model is

$$\begin{aligned} \dot{x} &= \mathcal{F}(x) + \mathcal{G}(T_J) \\ y &= \mathcal{H}(x) \\ S &= \mathcal{M}(y). \end{aligned} \quad (1)$$

The states $x = (m_0 \ m_1 \ m_2 \ m_3 \ T)^\top$ are the first four moments of the crystal size distribution [16] and the crystallizer temperature. The input is the jacket temperature T_J , the measured outputs $y = (T \ C)^\top$ are the crystallizer temperature and the concentration of the solute. The latter may be expressed as

$$C = C_i - \rho_c k_v (m_3 - m_{3,i}) \quad (2)$$

where C_i and $m_{3,i}$ are the initial values of C and m_3 , respectively. The control output S is the supersaturation, i.e. the difference between the concentration C and the solubility $C_s(T)$:

$$S = C - C_s(T) \quad (3)$$

where the solubility $C_s(T)$ is a third-order polynomial function of the temperature T

$$C_s(T) = a_0 + a_1 T + a_2 T^2 + a_3 T^3. \quad (4)$$

The state and the output mappings in (1) are given by

$$\mathcal{F}(x) = \begin{pmatrix} -\frac{UA}{\rho c_p V} T \\ k_b (C - C_s(T))^b m_3 \\ k_g (C - C_s(T))^g m_0 \\ 2k_g (C - C_s(T))^g m_1 \\ 3k_g (C - C_s(T))^g m_2 \end{pmatrix}, \mathcal{G}(T_J) = \begin{pmatrix} \frac{UA}{\rho c_p V} T_J \\ 0 \\ 0 \\ 0 \end{pmatrix}, \mathcal{H}(x) = \begin{pmatrix} T \\ C \end{pmatrix}, \quad (5)$$

$$\mathcal{M}(y) = C - C_s(T). \quad (6)$$

Note that S is given by the a static, nonlinear function $\mathcal{M}(y)$ of the measured output y .

system dynamics, and for this reason it is ignored in the modeling.

Symbol	Description	Value	Units
ρ_c	Crystal density	1130	kg/m ³
k_v	Crystal shape factor	0.1	-
ρ	Slurry density	789	kg/m ³
c_p	Slurry specific heat capacity	4185	J /(^o C kg)
V	Crystallizer volume	0.905	m ³
UA	Heat transfer coefficient · jacket area	$1.5 \cdot 10^5$	J /((min ^o C))
a_0	Solubility coefficient 0	27.8428	-
a_1	Solubility coefficient 1	2.0891	1/ ^o C
a_2	Solubility coefficient 2	-0.0311	1/ ^o C ²
a_3	Solubility coefficient 3	0.0017	1/ ^o C ³
k_g	Growth rate coefficient	$4.0 \cdot 10^{-4}$	m /min
g	Growth rate exponent	1.0	-
k_b	Nucleation rate coefficient	$1.57 \cdot 10^{13}$	1/(m ³ min)
b	Nucleation rate exponent	1.7	-

Table 1: Fixed coefficients and true parameters used in the data-generating system.

The initial concentration C_i and the initial state $x_i = (m_{0,i} \ m_{1,i} \ m_{2,i} \ m_{3,i} \ T_i)^\top$ are assumed to be fixed and known. The parameter vector $\beta = [k_g \ g]^\top$ contains the kinetic coefficients determining the growth behavior. In practice, these parameter are often subject to a large uncertainty. It is here assumed that a nominal parameter vector $\hat{\beta}_1$ is known a priori. However, the true parameter vector β_o used in the data-generating system (i.e. the model representing the true system in the simulation study) will differ from $\hat{\beta}_1$ in order to take the effect of *parametric model mismatches* into account. All the other symbols appearing in the model equations represent fixed coefficients and are assumed to be known exactly.³ The values of these fixed coefficients and the ones of the true parameters β_o used in the data-generating system are given in Table 1.

It will be convenient to consider the system in a finite, discrete-time representation. To this purpose, an ODE integration scheme with a fixed step $t_d = 5$ s is applied to the continuous-time system (1). After discretization, the

³In general, the coefficients k_b and b related to the nucleation are subject to large uncertainty. However, in the experimental conditions considered in this paper, these parameters have a very limited influence on the supersaturation dynamics. For this reason, they are fixed to their nominal value in the simulation model for simplicity.

batch time (assumed for simplicity to be equal for all the batches) corresponds to a certain number N of samples. For a certain input, output, or state variable V of the crystallization process, the bold-face symbol \mathbf{V} denotes a vector containing the N samples of V at the N discretization points. For instance, \mathbf{C} is the N -length vector containing the values of the concentration C at the discretization point. Furthermore, the notation $F_{WV}(\cdot)$ represents the mapping from the variable V to the variable W . Thus, for instance, the input/output dynamics $F_{CT_J}(\cdot)$ from T_J to C is denoted as $F_{CT_J}(\cdot)$, i.e. $\mathbf{C} = F_{CT_J}(\mathbf{T}_J)$. Note that such dynamics can be seen as the concatenation of a part $F_{TT_J}(\cdot)$ from T_J to T which is linear and fixed (first state equation in (5)), and a part $F_{CT}(\cdot)$ from T to C that is nonlinear and depends on the

uncertain parameters, i.e. $\mathbf{C} = F_{ST_J}(\mathbf{T}_J, \beta) = F_{ST}(\overbrace{F_{TT_J}(\mathbf{T}_J)}^{\mathbf{T}}, \beta)$ (see the two rightmost blocks in Figure 1).

Measurements \tilde{C} and \tilde{T} of C and T are collected at the same rate $t_s = t_d$ and corrupted by the noise signals e_C and e_T , respectively. The noise signals e_C and e_T are modeled as realizations of two independent white Gaussian processes having standard deviation $\sigma_T = 0.1$ °C and $\sigma_C = 0.002$ kg/kg, respectively. Furthermore, an additive disturbance δ_T is included on the crystallizer temperature in order to take into account the effect of unmodeled dynamics such as the thermal losses to the external environment, and the heat released due to the crystallization process. The disturbance δ_T is modeled as a first-order autoregressive process having standard deviation $\sigma_{AR} = 0.2$ °C:

$$\delta_T(t+1) = a\delta_T(t) + e(t) \quad (7)$$

where $a = 0.9895$ and $e(t)$ is white noise with standard deviation $\sigma_e = \sigma_{AR}\sqrt{1-a^2}$. The realizations of e_C, e_T and δ_T are different for all batches.

3. Batch-to-batch control algorithms

3.1. B2B+PI configuration

In order to cope with the disturbance δ_T on the temperature dynamics, a PI temperature controller is included in the control scheme. The B2B algorithm will be designed to update from batch to batch the reference trajectory T^r for the PI controller in order to track the supersaturation set-point S^r . The overall B2B+PI control scheme used in this paper is sketched in Figure 1. The two leftmost blocks in the scheme represent the control system:

the B2B supersaturation controller and the PI temperature controller. The signals coming and departing from the B2B block are updated off-line only, i.e. from batch to batch, and are indicated by dashed lines. All other signals are represented by continuous lines and are updated on-line during the same batch.

The different steps of the B2B+PI control approach are illustrated in a flowchart in Figure 2. After batch k is executed, the B2B controller uses the measurements in order to compute a temperature profile \mathbf{T}_{k+1}^r . This profile is used as reference for the PI controller during the next batch, and so on and so forth for the following ones. Note that the temperature profile \mathbf{T}_1^r corresponding to the first batch has to be fixed in advance. In practice, it may be set to an initial guess of the optimal temperature trajectory based on prior process knowledge.

PI temperature controller. The PI controller manipulates the jacket temperature T_J in such a way that the crystallizer temperature T follows the reference temperature T^r . The controller design is performed in the Laplace domain using a *model reference* approach aiming at a first-order closed loop transfer function from T^r to T in the form

$$T(s) = \frac{\overbrace{1}^{\mathbb{T}(s)}}{1 + st_{cl}} T^r(s), \quad (8)$$

where t_{cl} is the closed-loop time constant. Note that $\mathbb{T}(s)$ is the *complementary sensitivity function* of the control loop and is given by

$$\mathbb{T}(s) = \frac{L(s)}{1 + L(s)} \quad (9)$$

where $L(s)$ is the *loop transfer function*. From the model equations (5), the open-loop thermal dynamics from T_J to T in the Laplace domain is

$$T(s) = \frac{\overbrace{\frac{UA}{\rho c_p V}}^{G(s)}}{s + \frac{UA}{\rho c_p V}} T_J(s)$$

while the transfer function of the PI controller is $PI(s) = K_P + \frac{K_I}{s}$. The open loop transfer function is thus $L(s) = PI(s)G(s)$. Substituting this

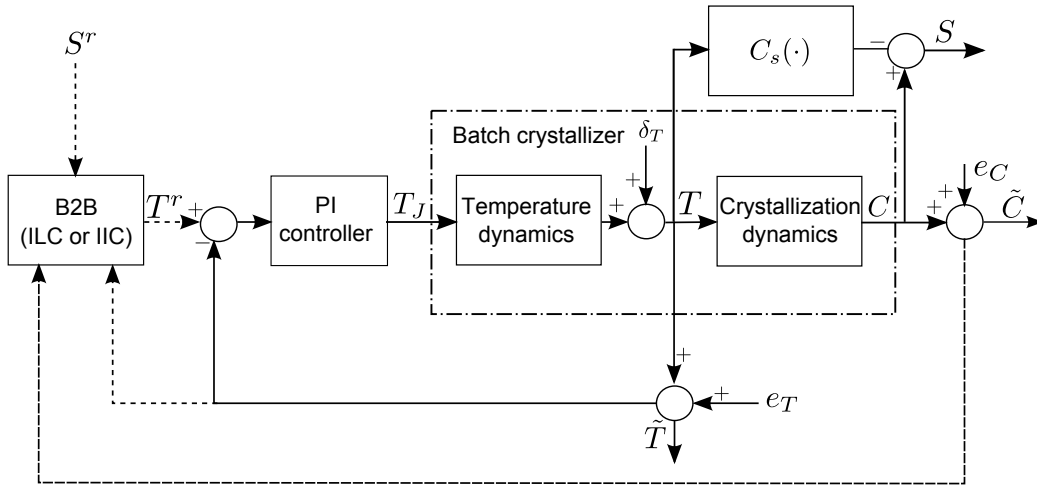


Figure 1: The B2B+PI control scheme. The B2B controller generates the reference T^r for the PI temperature controller in order to track the supersaturation reference S^r .

expression of $L(s)$ in (9) and equating the resulting expression to the desired complementary sensitivity function in (8), we find the required values for the coefficients of the PI controller $K_P = \frac{\rho c_p V}{t_{cl} U A}$ and $K_I = \frac{1}{t_{cl}}$. The closed-loop constant t_{cl} is set to 10 min. The resulting controller guarantees an effective rejection of δ_T and e_T , and a zero steady-state error in response to a constant temperature reference T^r owing to the presence of an integrator in the loop. A discrete-time version of this controller having sampling time $t_d = 5$ s is implemented in the simulation model: $PI(z) = K_P + t_d \frac{K_I}{z-1}$.

B2B supersaturation controller. After batch k , the corrupted measured outputs $\tilde{\mathbf{y}}_k = (\tilde{\mathbf{T}}_k, \tilde{\mathbf{C}}_k)^\top$ are available. The role of the B2B controller is to use this information to design an improved reference temperature profile \mathbf{T}_{k+1}^r for the PI controller in order to track the supersaturation reference \mathbf{S}_{k+1}^r in the batch $k+1$, i.e. to obtain a smaller supersaturation tracking error in the next batch (see Figure 1). The B2B algorithms ILC and IIC are described in details in the following subsections.

3.2. Iterative Learning Control

Different B2B control algorithms are categorized as ILC in literature [3]. In general, ILC algorithms may be defined as mappings that determine the input in the next batch based on a nominal process model and the input-

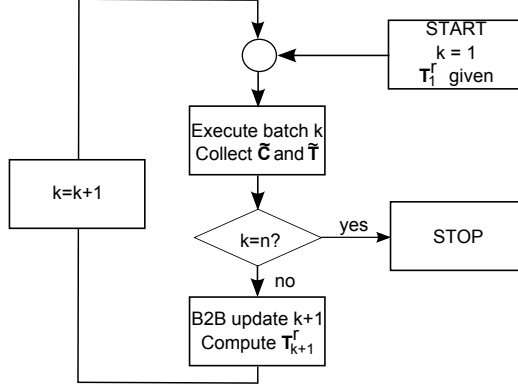


Figure 2: Flowchart of the B2B+PI control algorithm.

output data from previous batches in order to reduce the tracking error in the next batch.

The ILC algorithm presented here uses as nominal model the dynamics $F_{ST^r}(\cdot, \hat{\beta}_1)$ from the reference temperature T^r to the supersaturation S based on the nominal parameter vector $\hat{\beta}_1$.⁴ During the batch k , a certain temperature profile \mathbf{T}_k^r is given as reference to the PI controller, and the outputs $\tilde{\mathbf{y}}_k = (\tilde{\mathbf{T}}_k \tilde{\mathbf{C}}_k)^\top$ are collected. The ILC algorithm is used to design an improved temperature profile \mathbf{T}_{k+1}^r for the PI controller in order to track the supersaturation reference \mathbf{S}_{k+1}^r in the batch $k+1$.

Once the batch k is performed, the measurement $\tilde{\mathbf{y}}_k = (\tilde{\mathbf{T}}_k \tilde{\mathbf{C}}_k)^\top$ are first used to estimate the control output \mathbf{S}_k . The measurements are first filtered through a low-pass Butterworth filter $B(z)$ having cutoff frequency $1/t_f$ where $t_f = 5$ min. The filtering removes a good portion of the measurement noise, but it does not affect the underlying process dynamics, whose time constants are expected to be significantly larger than t_f . The filtered measurements $\tilde{\mathbf{y}}_{k,f} = (\tilde{\mathbf{T}}_{k,f} \tilde{\mathbf{C}}_{k,f})^\top$ are used to compute an estimate $\tilde{\mathbf{S}}_{k,f}$ of the supersaturation \mathbf{S}_k according to (6), i.e. $\tilde{\mathbf{S}}_{k,f} = \tilde{\mathbf{C}}_{k,f} - C_s(\tilde{\mathbf{T}}_{k,f})$.

Subsequently, an additive correction of the supersaturation model is performed using the estimated supersaturation $\tilde{\mathbf{S}}_{k,f}$. The ILC-updated model $\hat{S}_{k+1}^{\text{ILC}}(\cdot)$ of the dynamics from the reference temperature T^r to the supersat-

⁴ $\hat{\beta}_1$ is the best parameter estimate available before batch 1 is executed. Since in ILC model parameters are not updated from batch to batch, β_1 will also be used in the following steps of the algorithms.

uration S for the batch $k + 1$ is defined as

$$\hat{S}_{k+1}^{\text{ILC}}(\cdot) = F_{ST^r}(\cdot, \hat{\beta}_1) + \boldsymbol{\alpha}_{k+1} \quad (10)$$

where $\boldsymbol{\alpha}_{k+1}$ is the *correction vector* for the batch $k + 1$. The correction vector $\boldsymbol{\alpha}_{k+1}$ is an estimate obtained using $\tilde{\mathbf{S}}_{k,f}$ of the difference $\mathbf{S}_k - F_{ST^r}(\mathbf{T}_k^r, \hat{\beta}_1)$ (see later in this section for the exact definition of $\boldsymbol{\alpha}_{k+1}$). Let us assume now for simplicity that $\boldsymbol{\alpha}_{k+1}$ is exactly equal to $\mathbf{S}_k - F_{ST^r}(\mathbf{T}_k^r, \hat{\beta}_1)$. In this case, the output of the ILC-corrected model $\hat{S}_{k+1}^{\text{ILC}}(\cdot)$ in response to the reference temperature \mathbf{T}_k^r is equal to the output \mathbf{S}_k given by the data-generating system in response to the same reference temperature profile \mathbf{T}_k^r .

In ILC, the model (10) is used to optimize the reference temperature profile \mathbf{T}_{k+1}^r for the next batch according to the quadratic criterion

$$\mathbf{T}_{k+1}^r = \arg \min_{\mathbf{T}^r \in \mathbb{R}^N} \left\| \mathbf{S}_{k+1}^r - \hat{S}_{k+1}^{\text{ILC}}(\mathbf{T}^r) \right\|^2 \quad (11)$$

where \mathbf{S}^r is the supersaturation set-point.⁵

Note that, even in the ideal case where $\boldsymbol{\alpha}_{k+1} = \mathbf{S}_k - F_{ST^r}(\mathbf{T}_k, \hat{\beta}_1)$, the ILC-corrected model $\hat{S}_{k+1}^{\text{ILC}}(\cdot)$ is just an approximation of the data-generating system for the batch $k + 1$. In fact, the ILC-corrected model matches the output of the data-generating system only for the reference temperature \mathbf{T}_k^r , while the reference \mathbf{T}_{k+1}^r (obtained using (11)) will be applied in the batch $k + 1$. Nonetheless, the supersaturation output \mathbf{S}_{k+1} obtained by applying the reference profile \mathbf{T}_{k+1}^r is still expected to be closer to the set-point \mathbf{S}^r than \mathbf{S}_k .

⁵Problem (11) is solved numerically using the *active-set* method of the Matlab function `fmincon` and adopting a *single-shooting* dynamic optimization approach [2]. In order to reduce the dimensionality of the problem, the total length of \mathbf{T}^r is divided in $n_p = 40$ equally spaced intervals. \mathbf{T}^r is parametrized as a piecewise quadratic, continuous and differentiable function on the n_p intervals as in [5] and is thus determined by n_p optimization variables. Model equations are integrated at each optimization step in order to evaluate the objective as a function of the n_p optimization variables. The gradient of the objective function with respect to these optimization variables is obtained via finite differences. Note that such an approach is not guaranteed to find -in general- the global optimal solution of a non-linear, possibly non-convex optimization problem such as (11). However, in the simulations and in the experiments the optimization algorithm returned the same optimal value for different initialization of the optimization parameters. Thus, the result is likely to be close to the global optimum for the particular optimization problem at stake.

Therefore, after a number of batches, the supersaturation is expected to approach the desired set-point.

As suggested in [22], the correction vector is actually computed according to the quadratic criterion

$$\boldsymbol{\alpha}_{k+1} = \arg \min_{\boldsymbol{\alpha} \in \mathbb{R}^N} \left\| \tilde{\mathbf{S}}_{k,f} - (F_{ST^r}(\mathbf{T}_k^r, \hat{\beta}_1) + \boldsymbol{\alpha}) \right\|^2 + \lambda_k \|\boldsymbol{\alpha} - \boldsymbol{\alpha}_k\|^2. \quad (12)$$

The first term in (12) forces $\boldsymbol{\alpha}_{k+1}$ to be close to the difference $\tilde{\mathbf{S}}_{k,f} - F_{ST^r}(\cdot, \hat{\beta}_1)$. The second term in (12) has a regularization effect and prevents large variation for the correction vector $\boldsymbol{\alpha}_{k+1}$ with respect to the previous correction vector $\boldsymbol{\alpha}_k$. On the one hand, this regularization term is beneficial in order to reduce the influence of the noise affecting $\tilde{\mathbf{S}}_{k,f}$. On the other hand, the regularization term should not be too large because the actual difference $\mathbf{S}_{k,f} - F_{ST^r}(\mathbf{T}_k^r, \hat{\beta}_1)$ changes from batch to batch, since the reference temperature \mathbf{T}_k^r also changes from batch to batch. The scalar λ_k is a tuning parameter, possibly iteration-dependent, which represents a trade-off between the two objectives.

3.3. Iterative Identification Control

In the IIC algorithm, the measurements $\tilde{\mathbf{y}}_k = (\tilde{\mathbf{T}}_k \tilde{\mathbf{C}}_k)^\top$ collected from one batch are used to update an estimate $\hat{\beta}_{k+1} \triangleq [\hat{k}_{g,k+1} \hat{g}_{k+1}]$ of the unknown parameter vector β_o . The IIC-updated model from the reference temperature T^r to the supersaturation S for the batch $k+1$ is defined as

$$\hat{S}_{k+1}^{\text{IIC}}(\cdot) = F_{ST^r}(\cdot, \hat{\beta}_{k+1}). \quad (13)$$

The estimation of the parameter $\hat{\beta}_{k+1}$ is performed iteratively in a Maximum a Posterior (MAP) framework [20], which combines the previous estimate $\hat{\beta}_k$ with the data $\tilde{\mathbf{y}}_k = [\tilde{\mathbf{T}}_k \tilde{\mathbf{C}}_k]^\top$ measured in the current batch. By doing this, the variance of the estimated parameters decreases after each batch since the estimation is performed using an increasing amount of information. Using the notation introduced in Section 2, the dynamics of the data-generating system from T to C is described by the mapping $F_{CT}(\cdot, \beta)$ with $\beta = \beta_o$.

An approximation of the MAP estimator for this problem is given by ⁶

$$\hat{\beta}_{k+1} = \arg \min_{\beta} \frac{1}{\sigma_C^2} \left\| \tilde{\mathbf{C}}_k - F_{CT}(\tilde{\mathbf{T}}_k, \beta) \right\|^2 + \left\| \beta - \hat{\beta}_k \right\|_{P_k^{-1}}^2. \quad (14)$$

⁶Formally, an Errors-in-Variables (EIV) estimation problem [19] should be solved since both $\tilde{\mathbf{T}}_k$ and $\tilde{\mathbf{C}}_k$ are corrupted by measurement noise. However, computing the MAP esti-

where $F_{CT}(\cdot, \beta)$ is the uncertain dynamics from T to C , the matrix P_k for $k \geq 2$ is the covariance matrix of the estimated parameter vector $\hat{\beta}_k$ (the covariance matrices will also be iteratively estimated, see later). Since there is no covariance matrix associated with $\hat{\beta}_1$, the matrix P_1^{-1} is set to 0 in our algorithm. By doing so, $\hat{\beta}_1$ has no influence on the estimates $\hat{\beta}_k$, $k \geq 2$.⁷

When the data-generating system belongs to the assumed model structure $F_{CT}(\cdot, \beta)$, the estimated parameter vector $\hat{\beta}_{k+1}$ is asymptotically⁸ normally distributed around β_o with a covariance matrix P_{k+1} given by

$$P_{k+1}^{-1} = P_k^{-1} + \frac{1}{\sigma_C^2} \overbrace{\frac{\partial F_{CT}(\mathbf{T}_k, \beta)}{\partial \beta}^\top \frac{\partial F_{CT}(\mathbf{T}_k, \beta)}{\partial \beta}}^{I_k} \Bigg|_{\beta=\beta_o} \quad (15)$$

where $I_k \geq 0$ is the *information matrix* related to the experiment k . In practice, the true parameter β_o and the noise-free temperature \mathbf{T}_k are not known. Therefore, the information matrix is here approximated as

$$\tilde{I}_k = \frac{1}{\sigma_C^2} \frac{\partial F_{CT}(\tilde{\mathbf{T}}_k, \beta)}{\partial \beta}^\top \frac{\partial F_{CT}(\tilde{\mathbf{T}}_k, \beta)}{\partial \beta} \Bigg|_{\beta=\hat{\beta}_k}, \quad (16)$$

i.e. the derivatives of $F_{CT}(\mathbf{T}_k, \beta)$ with respect to the parameter vector β are computed in $\hat{\beta}_k$ instead of the unknown β_o , and the noisy signal $\tilde{\mathbf{T}}_k$ is used instead of \mathbf{T}_k .

Finally, the updated model $S_{k+1}^{\text{IIC}}(\cdot)$ is used to design the temperature profile for the next batch as

$$\mathbf{T}_{k+1}^r = \arg \min_{\mathbf{T}^r \in \mathbb{R}^N} \left\| \mathbf{S}_{k+1}^r - \hat{S}_{k+1}^{\text{IIC}}(\mathbf{T}^r) \right\|^2. \quad (17)$$

mator for an EIV problem is rather complicate, in particular for a generic nonlinear system such as the one describing the batch cooling crystallization process. The approximated formula (14) is rigorously valid only in the case $\tilde{\mathbf{T}}_k = \mathbf{T}_k$, i.e. in absence of temperature measurement noise. Nonetheless, the authors verified from numerical simulations that effect of this approximation is negligible for typical values of temperature measurement noise.

⁷A covariance matrix P_1 may be available when $\hat{\beta}_1$ is obtained from a preliminary identification step. In that case, P_1^{-1} could be initialized using that covariance matrix.

⁸In the number N of samples.

Remark 1. *In IIC, the inverse P_k^{-1} of the parameter covariance matrix increases from batch to batch by a term that corresponds to the information matrix I_k (see Equation (15)). Thus, the covariance of the estimated parameters decreases significantly only if the information matrix is sufficiently large. This condition could be enforced for instance by superposing a specially tailored excitation signal on top of reference temperature profile T^r (see [10]). However, such an excitation signal would also decrease the supersaturation tracking performance when it is applied, since it would act as an additional disturbance on the system. In our case, it was found that the reference temperature profile T^r generated according to (17) leads to a sufficiently large information matrix. For this reason, we did not consider the use of excitation signals in the IIC algorithm.*

Summarizing, in the ILC and the IIC algorithms these steps are executed for each batch k :

1. The reference temperature \mathbf{T}_k^r is set as the input to the temperature controller. The batch k is performed and the noisy measurements $\tilde{\mathbf{y}} = (\tilde{\mathbf{T}}_k, \tilde{\mathbf{C}}_k)^\top$ are collected.
2. A corrected model $\hat{S}_{k+1}(\cdot)$ of the dynamics from T^r to S is obtained according to the ILC criterion (10) or the IIC criterion (13), respectively.
3. The corrected model is used to compute the temperature profile for the next batch according to (11) in ILC or (17) in IIC.

Remark 2. *The model update performed in ILC to obtain α_{k+1} (12) and in IIC to obtain β_{k+1} (14) have a very similar structure. They are both defined as the solution of a multi-objective optimization problem aiming at fitting the most recent dataset, while limiting the model change with respect to the previous batch. However, while in IIC the optimization problem is formally derived as the MAP solution of an estimation problem formulated in a stochastic framework, in ILC it is introduced using an intuitive argument. In [4], the authors introduced a stochastic framework for ILC that allows one to obtain the correction vector α_{k+1} as the result of a MAP estimation procedure. This approach can ease the tuning of the ILC algorithm, i.e. the choice of the parameter λ_k . However, we do not present this approach in detail in this paper since (i) it would require the introduction of further concepts and notational complexity and (ii) the technique was not used in the experimental campaign. The interested reader is referred to [4].*

4. Simulation Results

In this section, the performance of the B2B scheme on two different simulation cases is evaluated, namely in the presence of parametric model mismatches only (Case 1) and in the presence of parametric and structural mismatches (Case 2). The batch time is $t_f = 150$ min and the total number of batches is $n = 20$. The desired supersaturation is the constant value $\mathbf{S}^r = 0.0028$ kg/kg for all the batches. The reference temperature for the first batch \mathbf{T}_1^r is set to a linear cooling trajectory from 45 to 22.5 °C in the time interval $[0, t_f]$. The corresponding supersaturation is far from the set-point (Figure 3, Batch 1).

For the ILC algorithm, the tuning parameter λ_k is set to 0 for $k = 1, \dots, 5$ and to 4 for $k = 6, \dots, 20$. This choice of is adopted because in the first batches a significant change in the reference temperature is expected, and adapting the correction vector in order to match the previously measured supersaturation is considered more important than rejecting the measurement noise. Therefore, λ_k is kept to zero. Afterwords, the change of the reference temperature is expected to be lower and λ_k is increased in order to further improve the tracking performance by filtering the noise from estimate of the correction vector.

4.1. Case 1

The performance of the algorithms in presence of parametric model mismatch is evaluated. The data-generating system is constructed based on the system equations (1)-(5) with the true parameter vector $\beta_o = [4 \cdot 10^{-4} \ 1]^\top$, while the nominal parameter vector $\hat{\beta}_1 = [5 \cdot 10^{-4} \ 1.1]^\top$ is used in the design of the ILC algorithms.

The simulation results are shown in Figure 3. For batches 1, 2, 3, and 20 the reference temperature profile T_k^r , the supersaturation S_k , and the supersaturation set-point S^r are reported. In the case of ILC, we also report the correction vector α_k . In Batch 2 the tracking error is already small for IIC, while it is still appreciable for ILC. This confirms the intuition that IIC can be more efficient than ILC, at least in the case when the model structure used for parameter estimation can describe the data-generating system (see later). After some iterations, also ILC approaches the set-point more closely (Batch 10). Note also that the correction vector α_k is smoothed through the iterations owing to larger value of the tuning parameter λ_k .

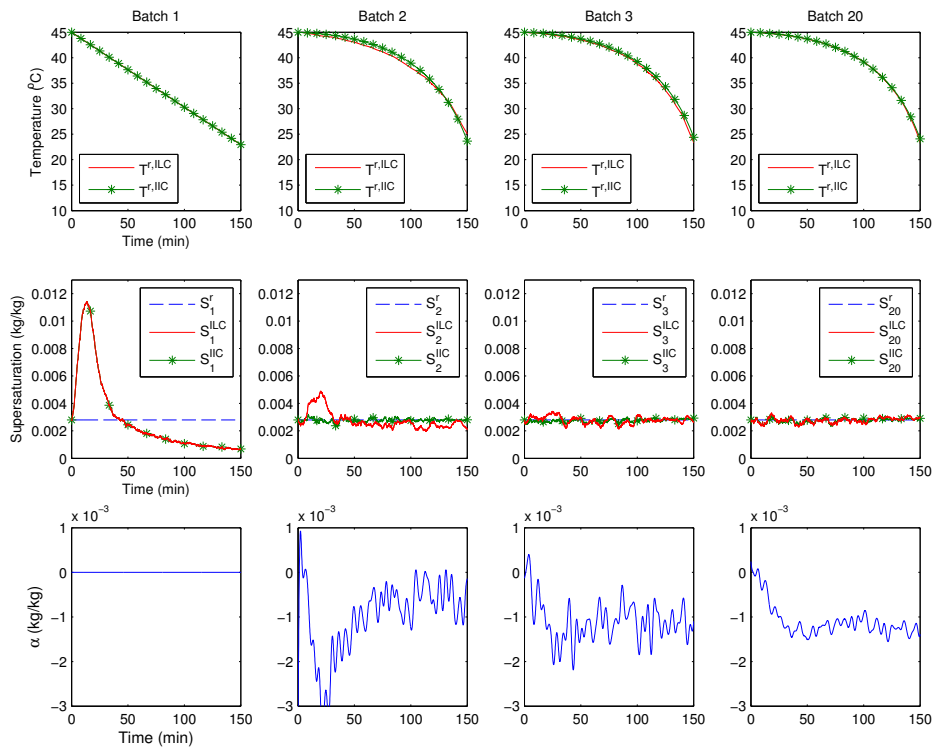


Figure 3: Case 1: reference temperature T^r and supersaturation S for the batches 1,2,3,20.

4.2. Case 2

In addition to the parametric mismatch, Case 2 considers a structural model mismatch. A temperature-dependent crystal growth mechanism is introduced in the data-generating system. The state equations 2,3,4 in the state-space map (5) are multiplied by the term $A_0 \exp(-E_a/R(T + K_0))$, with $A_0 = 1.0 \times 10^7$, $E_a = 4.2 \times 10^4$ J/mol, $R = 8.3144$ Jmol/ · K and $K_0 = 273.15$ °C. The modified state-space mapping is

$$\tilde{\mathcal{F}}(x) = \begin{pmatrix} k_b(C - C_s(T))^b m_3 \\ A_0 \exp(-E_a/R(T + K_0)) k_g (C - C_s(T))^g m_0 \\ A_0 \exp(-E_a/R(T + K_0)) 2k_g (C - C_s(T))^g m_1 \\ A_0 \exp(-E_a/R(T + K_0)) 3k_g (C - C_s(T))^g m_2 \\ -\frac{UA}{\rho c_p V} T \end{pmatrix} \quad (18)$$

However, the B2B algorithms are still based on the nominal state-space mapping (5). The results of the simulations are reported in Figure 4. As in Case 1, the reference temperature profile T_k^r , the supersaturation S_k , and the supersaturation set-point S^r are reported for the batches 1, 2, 3, and 20. In the case of ILC, the correction vector α_k is also reported.

The IIC algorithm leads to a rather poor tracking performance in all the batches. Apparently, due to the structural model mismatch the estimated models cannot represent the dynamics of the data-generating system with a sufficient accuracy in order to track the desired supersaturation set-point. On the contrary, the ILC algorithm is still capable of approaching the set-point, even though more iterations than in the Case 1 are required. The general model correction performed using the correction vector α_k is indeed more suitable to compensate the nominal model for structural model mismatches.

4.3. Discussion on the simulation results

The Root Mean Square (RMS) of the supersaturation tracking error is plotted against the batch number for all cases in Figure 5. The different behavior of the two algorithms is evident in this plot. IIC provides the best performance when the model structure selected can describe the data-generating system. A good result is already obtained after the first iteration of the algorithm. However, the behavior of the algorithm is hard to predict (and the performance is in general lower) in the case of structural model mismatches. The IIC framework indeed strongly relies on the assumption of the model structure. In the situation considered where an

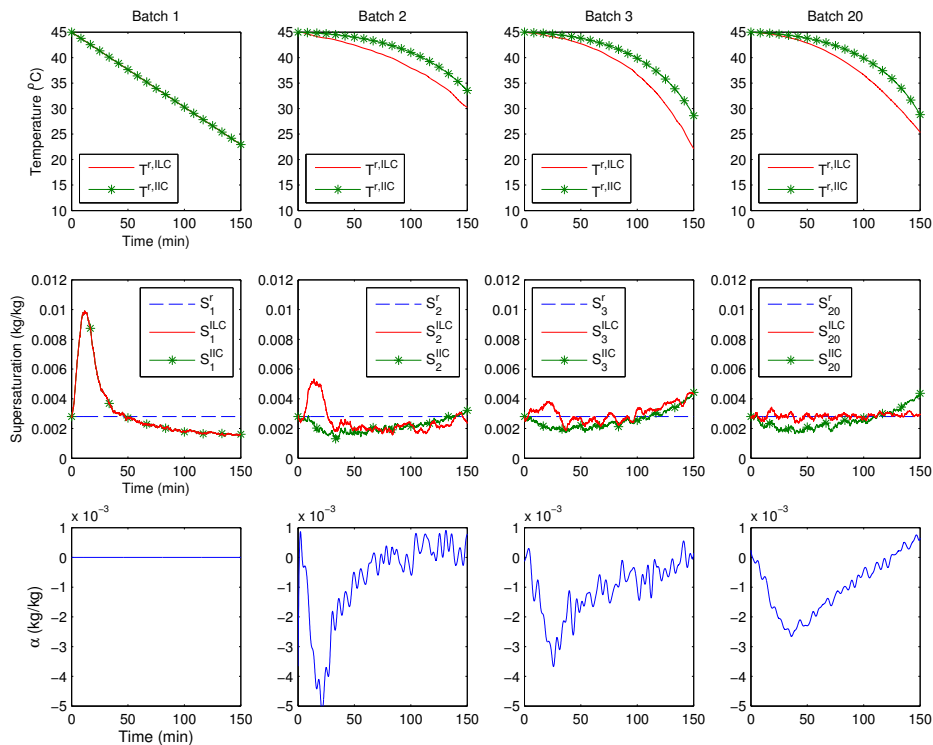


Figure 4: Case 2: reference temperature T^r and supersaturation S for the batches 1,2,3,10

unmodeled temperature-dependent growth behavior is incorporated in the data-generating system, IIC leads to a worse overall performance compared to ILC. Indeed, ILC is much more robust to structural model mismatches due to the non-parametric model correction. Even though these mismatches make the convergence somewhat slower, a satisfactory set-point tracking is eventually achieved. In this sense, in order to fully benefit from the B2B approach it would be useful to design an additional control layer suggesting the most appropriate model update strategy for the next batch (i.e. IIC or ILC) based on the results obtained in the previous batches. Ideas in this direction may be found in the field of Supervisory Control [13].

5. Experimental Results

In this section, the results of the batch-to-batch supersaturation control experiments performed on a pilot-scale batch cooling crystallizer are presented. A schematic representation of the experimental setup is given in

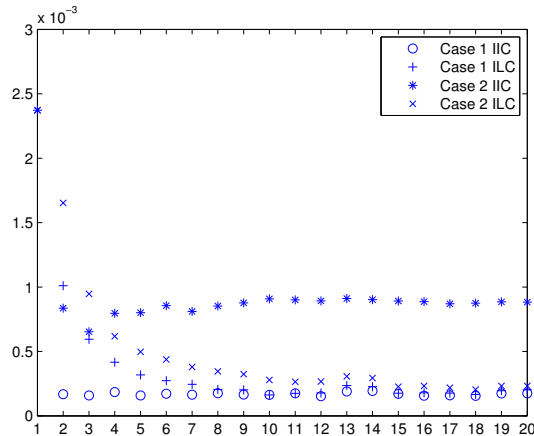


Figure 5: RMS of the supersaturation tracking error vs batch number for IIL and ILC in Case 1 and 2.

Figure 6. The crystallizer is a 50-liter, jacketed glass vessel (Figure 7). An impeller is used to agitate the content of the crystallizer and ensure that the suspension is well mixed. The temperature in the crystallizer is manipulated by circulating a cooling medium (a solution of water and glycol) in the jackets of the vessel. A thermostatic bath (LAUDA RUK 90 S) is used to heat up and cool down this cooling medium. The same thermostatic bath is equipped with a pump that allows the circulation of the cooling medium in the jackets.

The measurements are collected using a skid platform that is described in detail in [8]. The skid platform consists of two separate pieces of equipment called pump skid and instrument skid, respectively. The crystal slurry is circulated from the bottom valve of the crystallizer to the pump skid, from the pump skid to an instrument skid, and finally back to the top of the crystallizer with the help of a lobe pump (Omac BF330) mounted on the pump skid. Different sensors can be mounted inside the instrument skid in order to collect measurements from the liquid and/or the solid phase of the slurry. In this work, the K-Patents PR-23 refractometer was used. By measuring the refractive index (and through a previous calibration of the instrument), it is possible to reconstruct the concentration C of the solute dissolved in the liquid phase [17]. Two PT100 temperature sensor are also mounted inside the thermostatic bath and inside the vessel in order to measure the jacket temperature T_J and the crystallizer temperature T , respectively. The control

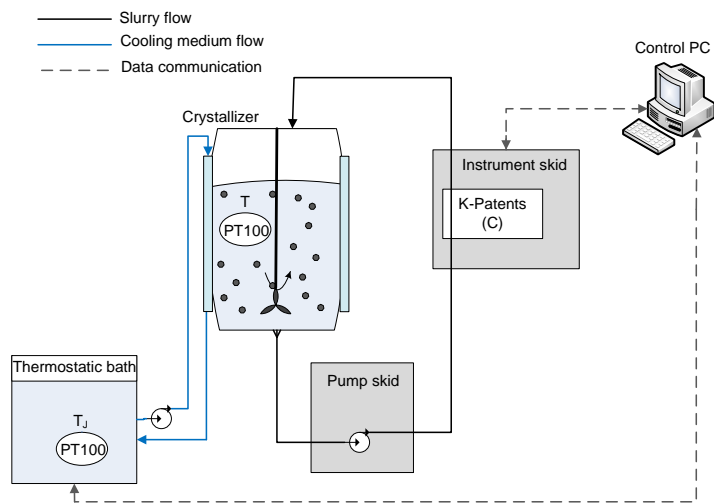


Figure 6: A schematic representation of the experimental setup.

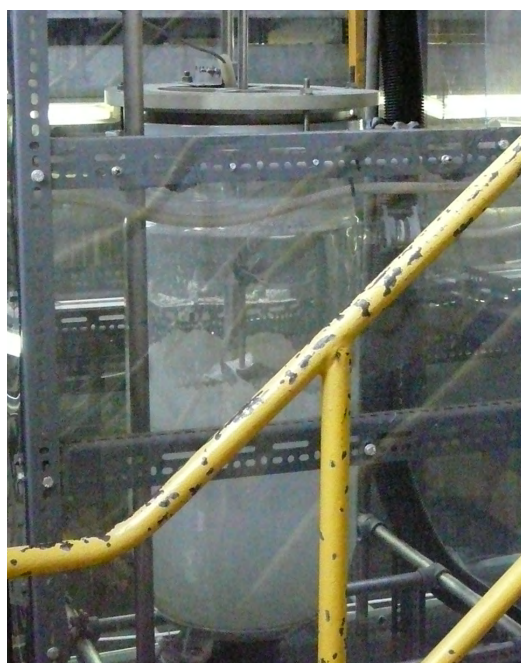


Figure 7: The 50-liter crystallizer used in the experiments.

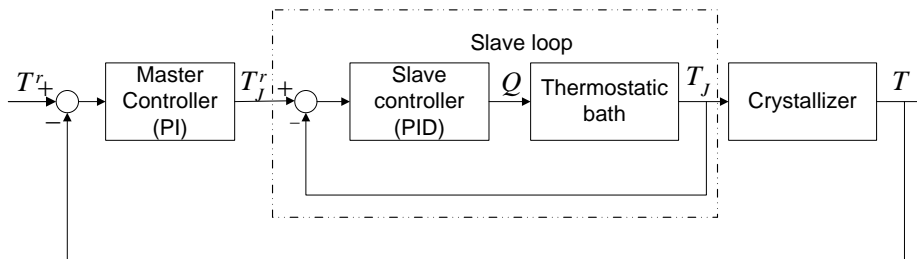


Figure 8: The master-slave temperature control scheme.

tasks are performed on the Control PC that communicates with the instrument skid (and with the thermostatic bath) using the OPC communication protocol.

The crystallization compound is Succinic acid dissolved in water. A small amount of Fumaric acid was also added in order to simulate the presence of impurities, which are very common in industrial crystallization processes. The crystallizer was initially loaded with 45.2 kg of water, 8.6 kg of Succinic acid, and 0.4 kg of Fumaric acid.

5.1. Temperature control architecture

The temperature inside the crystallizer was controlled using the master-slave control configuration represented in Figure 8. A lower-level slave PID controller (which is directly integrated in the thermostatic bath) was used to regulate the jacket temperature T_J in order to follow the set-point T_J^r . The default factory settings for this PID were found to be satisfactory and were not modified. The dynamics of the slave loop were found to be much faster (in the order of few minutes) than the ones of the temperature in the crystallizer (in the order of an hour).

A higher-level master PI controller (implemented on the Control PC) was designed in order to provide the set-point T_J^r to the slave PID controller in such a way that the crystallizer temperature T follows the reference T^r . Note that the slave loop was ignored in the simulation model presented in Section 3.1. The master PI controller in Figure 8 corresponds in fact to the PI controller in Figure 1, while the slave loop is not present in Figure 1, since it was assumed for simplicity that $T_J^r = T_J$.

The design of the master PI controller was performed similarly to the design of the PI controller presented in Section 3.1. Based on the linear model

of the temperature dynamics $T = \frac{2.925 \cdot 10^{-4}}{s+2.53 \cdot 10^{-4}} T_J$, which was previously identified with the Matlab System Identification Toolbox [11] using experimental data, the master PI controller $PI(s) = \frac{5.698(s+2.53 \cdot 10^{-4})}{s}$ was designed. The resulting closed-loop system from T^r to T has a linear, first-order behavior with a time constant $t_{cl} = 10$ min

$$T = F_{TT^r}(s) = \frac{1}{1 + \frac{s}{600}} T^r. \quad (19)$$

The actual command T_J^r was generated by a discrete-time version of the controller $PI(s)$, and was limited in the range $[5 - 90 \text{ }^\circ\text{C}]$ for safety considerations.

5.2. Batch-to-batch supersaturation control experiments

A total of four batch cooling crystallization experiments were performed. The first two experiments were performed to estimate a nominal process model and to find a suitable supersaturation set-point. In the next two experiments, the supersaturation was controlled using the ILC algorithm presented in Section 3.

The time profiles of temperature and supersaturation for the four experiments is shown in Figure 9. For all the experiments, seeding [9] was applied at the time instant $t = 0$ using 0.005 kg of milled Succinic acid crystals having a mean size of $25 \mu\text{m}$ in order to initialize the process with a fixed crystal size distribution. The duration of a batch is $t_f = 150$ min. We aimed at initial values of temperature and concentration of $T_i = 45 \text{ }^\circ\text{C}$ and $C_i = 0.1731 \text{ kg/kg}$, respectively. The corresponding initial value for the supersaturation is $S_i = C_i - C_s(T_i) = 0.0034 \text{ kg/kg}$.

Two metrics are considered in order to compare the outcome of the experiments: the maximum value of the supersaturation during the experiment, and the RMS of the supersaturation tracking error.

Experiment 1: preliminary model estimation. The crystallizer was cooled from $45 \text{ }^\circ\text{C}$ to $22.5 \text{ }^\circ\text{C}$ in 150 min following an approximately linear temperature trajectory. The objective of this experiment was to collect data in order to build a preliminary process model.

The time profiles of crystallizer temperature T_1 and of the supersaturation S_1 are reported in Figure 9 (Experiment 1). The measurements of temperature and concentration obtained from this experiment were used in order to

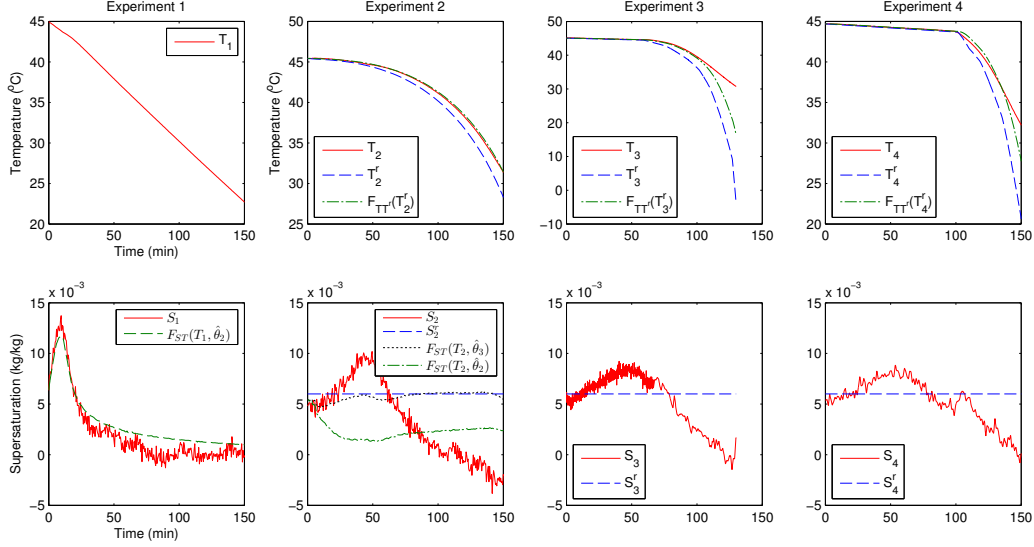


Figure 9: Temperature and supersaturation of the four experiments.

estimate the kinetic parameters of the model. The parameters estimated according to (14) were $\hat{\beta}_2 = [\hat{k}_{g,2} \hat{g}_2]^\top = [6.77 \cdot 10^{-4} \ 1.05]^\top$. The supersaturation output $F_{ST}(T_1, \hat{\beta}_2)$ of the model $F_{ST}(\cdot, \hat{\beta}_2)$ fed by the measured temperature T_1 is also shown in the supersaturation plot for this experiment. This model is able to describe the supersaturation dynamics of the experiment rather accurately.

The model $F_{ST}(\cdot, \hat{\beta}_2)$ was complemented with the model of the closed-loop temperature dynamics $F_{TT^r}(\cdot)$ given by (19), and a model $F_{ST^r}(\cdot, \hat{\beta}_2)$ from the reference temperature T^r to the supersaturation S was obtained: $F_{ST^r}(\cdot, \hat{\beta}_2) = F_{ST}(F_{TT^r}(\cdot), \hat{\beta}_2)$.

Experiment 2: model validation and set-point selection. The crystallizer was cooled down 45 °C to 27 °C following a parabolic-like temperature trajectory.⁹ The objective of Experiment 2 was twofold. The first aim is to evaluate the predictive capability of the model $F_{ST^r}(F_{TT^r}(\cdot), \hat{\beta}_2)$ obtained from the data of Experiment 1 in response to a different reference temperature trajectory. The

⁹This trajectory was obtained by optimizing the model $F_{ST^t}(F_{TT^r}(\cdot), \hat{\beta}_2)$ in order to follow the constant supersaturation set-point $S^r = 0.0028$ kg/kg. The latter was determined as the average of the supersaturation in the first two hours of Experiment 1.

second aim is to find a suitable supersaturation set-point for the following experiments.

The time profiles of the reference temperature T_2^r , the measured temperature T_2 , the temperature model $F_{TT^r}(T_2)$, and the supersaturation S_2 for this experiment are shown in Figure 9 (Experiment 2). The temperature T_2 is described very accurately by the model $F_{TT^r}(T_2)$ for most of the batch time and drifts slightly away in the final 10 minutes of the experiment, indicating that the constraint on the maximum cooling power of the thermostatic bath is reached. Thus, apart from the small deviation due to the actuator limitations, the temperature dynamics is accurately described by the model $F_{TT^r}(T_2)$. Conversely, the supersaturation S_2 is very far from the output $F_{ST}(T_2, \hat{\beta}_2)$ given by the previously estimated model. For this reason, the measurements of temperature and concentration from this experiment were used to compute new estimates for the parameters k_g and g . The newly estimated parameters were $\hat{\beta}_3 = [\hat{k}_{g,3} \hat{g}_3]^\top = [1.78 \cdot 10^{-4} \ 1.00]^\top$.

The output $F_{ST}(T_2, \hat{\beta}_3)$ of the new model is also shown in Figure 9 (Experiment 2). Note that not even the model $F_{ST}(T_2, \hat{\beta}_3)$ estimated using the data of Experiment 2 interpolates the actual supersaturation S_2 accurately. Apparently, the actual process dynamics are more complicated than the ones that our model structure can describe. In other words, there is a significant structural model mismatch. In order to compensate for the structural model mismatch in the next batch-to-batch control experiments, ILC model corrections were applied for the following experiments.

In Experiment 2, the supersaturation S_2 reached a maximum value of approximately 0.01 kg/kg around time 50 min. In general, too high values for the supersaturation have to be avoided since they could lead to a degradation of the quality of the produced crystals. Our objective for the following experiments was to reduce the peak of the supersaturation. In order to achieve this, the supersaturation set-point $S^r = 0.006$ kg/kg was selected in the following experiments. The RMS of the supersaturation tracking error for Experiment 2 with respect to the set-point $S^r = 0.006$ kg/kg is 0.0057 kg/kg.

Experiment 3: tracking of $S^r = 0.006$ kg/kg using ILC. In order to account for the structural model mismatch observed in Experiment 2, an ILC correction based on the model $F_{ST^r}(\cdot, \hat{\beta}_3) = F_{ST}(F_{TT^r}(\cdot), \hat{\beta}_3)$ was performed. The correction vector α_3 was computed as $\alpha_3 = B(z)(S_2 - F_{ST^r}(T_2, \hat{\beta}_3))$ where S_2 is the measured output from the previous experiment and $B(z)$ is the low-pass Butterworth filter introduced in Section 2. The updated model

$F_{ST}(\cdot, \hat{\beta}_3) + \alpha_3$ was used to optimize the reference temperature T_3^r in order to track the reference $S^r = 0.006$ kg/kg. The time profiles of the reference temperature T_3^r , the measured temperature T_3 , the temperature model $F_{TTr}(T^r)$, and the supersaturation S_3 for this experiment are shown in Figure 9 (Experiment 3). The RMS of the supersaturation tracking error is significantly reduced, from 0.0057 kg/kg of the B2B experiment 2 to 0.0029 kg/kg. Furthermore, the maximum of the supersaturation is also slightly reduced, from 0.01 kg/kg of Experiment 2 to 0.008 kg/kg.

Note that the reference temperature T_3^r decreases very slowly for the first part of the experiment, and much faster towards the end. However, the actual crystallizer temperature cannot decrease as fast as required due to the limitations of the thermostatic bath (and T_3 moves away from the model $F_{TTr}(T_3^r)$). Therefore, the supersaturation S_3 drops below the set-point (and very close to zero) towards the end of the batch.

Experiment 4: tracking of $S^r = 0.006$ kg/kg using ILC. A final experiment was performed with the same set-point $S^r = 0.006$ kg/kg. An ILC model update from the B2B experiment 3 was applied. The correction vector α_4 was computed as $\alpha_4 = B(z)(S_3 - F_{STr}(T_3, \hat{\beta}_3))$, and the ILC-updated model $F_{STr}(\cdot, \hat{\beta}_3) + \alpha_4$ was used to design the reference temperature T_4^r . The time profiles of the reference temperature T_4^r , the measured crystallizer temperature T_4 , the temperature model $F_{TTr}(T_4)$ and the supersaturation S_4 for this experiment are shown in Figure 9 (B2B experiment 4). The RMS of the supersaturation tracking error is further reduced, from 0.0029 kg/kg in the B2B experiment 3 to 0.0025 kg/kg. The maximum of the supersaturation is around 0.008 kg/kg, as in Experiment 3.

5.3. Discussion on the experimental results

The B2B control framework enables reducing the supersaturation tracking error and lowering the maximum value of the supersaturation. Even though we did not perform a thorough particle analysis of the crystals produced (in terms e.g. of crystal size distribution, morphology, etc.), the improved supersaturation control is expected to lead to a better quality [15]. The results of these experiments are promising, but further work is still required in order to bring similar B2B control strategies to an industrial production environment.

First, achieving a constant supersaturation seems to be an unfeasible objective for this crystallization process since towards the end of the batch

a very fast cooling rate is required. In practice, this temperature trajectory cannot be implemented due to limitations on the actuator. Therefore, it may be debated whether a different control objective could be chosen.

Second, it was observed that there is a severe structural mismatch between the available crystallization model and the actual process dynamics. This prevented us from using the IIC strategy, which potentially could lead to a faster learning of the optimal temperature trajectory.

In order to overcome the issues caused by the structural model mismatch, ILC model corrections were applied. However, a difficulty in the implementation of ILC is that the algorithm requires the same initial conditions for all the batches. We found that bringing the system to the same initial condition is a rather involved procedure even for a pilot-scale setup, and it would hardly be possible to incorporate into the industrial practice. In this sense, it would be useful to develop ILC strategies that are guaranteed to be robust to variations in the initial condition.

6. Conclusions

A batch-to-batch framework for the control of supersaturation in a batch cooling crystallization process has been presented. The batch-to-batch controller designs a temperature trajectory in order to track a given supersaturation reference. The temperature trajectory determined by the batch-to-batch controller is given as reference to the PI temperature controller, whose main role is to reject the real-time disturbances on the temperature dynamics. Two batch-to-batch algorithms are examined in this paper, namely Iterative Learning Control (ILC) and Iterative Identification Control (IIC).

The simulation results indicate that the algorithms have complementary advantages and disadvantages. On the one hand, IIC provides the best performance when the assumed model structure can describe the data-generating system. However, the performance of IIC is hard to predict (and generally lower) when the true system is not contained in the assumed model structure, i.e. in the case of structural model mismatches. On the other hand, ILC is more robust to structural model mismatches. Even though these mismatches slow down the convergence, a satisfactory result is eventually obtained after a number of batches. From a theoretical perspective, it would be attractive to proof these properties observed in simulation in rigorous and possibly quantitative terms. Such a theoretical background would also be useful for the design of a supervisory control layer suggesting at each step which of the two

algorithms should be used. Note however that developing this knowledge is a tough challenge due to the inherently non-linear nature of the crystallization process.

Experiments were performed to apply the ILC algorithm to a real pilot-scale crystallization setup. The results of these experiments are promising. The supersaturation tracking error and the maximum value of the supersaturation were lowered in three batches. Even though a number of issues still have to be solved, the authors expect that in the near future similar B2B control strategies could be applied for this process in industrial production environments.

References

- [1] M. Barrett, M. McNamara, H. Hao, P. Barrett, and B. Glennon. Supersaturation tracking for the development, optimization and control of crystallization processes. *Chemical Engineering Research and Design*, 88(8):1108–1119, 2010.
- [2] T. Binder, L. Blank, H.G. Bock, R. Bulirsch, W. Dahmen, M. Diehl, T. Kronseder, W. Marquardt, J.P. Schlöder, and O. von Stryk. Introduction to model based optimization of chemical processes on moving horizons. In *Online optimization of large scale systems*, pages 295–339. Springer, 2001.
- [3] D.A. Bristow, M. Tharayil, and A.G. Alleyne. A survey of iterative learning control. *Control Systems Magazine, IEEE*, 26(3):96–114, 2006.
- [4] M. Forgione, A. Mesbah, X. Bombois, and P.M.J. Van den Hof. Batch-to-batch strategies for cooling crystallization. In *Proceedings of the 51st IEEE Conference on Decision and Control (CDC)*, pages 6364–6369, 2012.
- [5] M. Forgione, A. Mesbah, X. Bombois, and P.M.J. Van den Hof. Iterative learning control of supersaturation in batch cooling crystallization. In *Proceedings of the 2012 American Control Conference, Fairmont Queen Elizabeth, Montreal, Canada*, pages 6455–6460, 2012.
- [6] M. Fujiwara, Z.K. Nagy, J.W. Chew, and R.D. Braatz. First-principles and direct design approaches for the control of pharmaceutical crystal-

- lization. *Journal of Process Control*, 15(5):493–504, 2005. ISSN 0959-1524.
- [7] T. Gutwald and A. Mersmann. Batch cooling crystallization at constant supersaturation: technique and experimental results. *Chemical Engineering & Technology*, 13(1):229–237, 1990.
- [8] S.S. Kadam, J.A.W. Vissers, M. Forgione, R.M. Geertman, P.J. Daudey, A.I. Stankiewicz, and H.J.M. Kramer. Rapid crystallization process development strategy from lab to industrial scale with pat tools in skid configuration. *Organic Process Research & Development*, 16(5):769–780, 2012.
- [9] A.N. Kalbasenka, L.C.P. Spierings, A.E.M. Huesman, and H.J.M. Kramer. Application of seeding as a process actuator in a model predictive control framework for fed-batch crystallization of ammonium sulphate. *Particle & Particle Systems Characterization*, 24(1):40–48, 2007.
- [10] L. Ljung. *System identification*. Englewood Cliffs, NJ: Prentice-Hall, 1999.
- [11] L. Ljung. System identification toolbox. For Use with MATLAB, 2007.
- [12] A. Mesbah, Z.K. Nagy, A.E.M. Huesman, H.J.M. Kramer, and P.M.J. Van den Hof. Nonlinear model-based control of a semi-industrial batch crystallizer using a population balance modeling framework. *Control Systems Technology, IEEE Transactions on*, 20(5):1188–1201, 2012.
- [13] A.S. Morse. Supervisory control of families of linear set-point controllers part i. exact matching. *Automatic Control, IEEE Transactions on*, 41(10):1413–1431, 1996.
- [14] A.S. Myerson. *Handbook of industrial crystallization*. Butterworth-Heinemann, 2002.
- [15] Z.K. Nagy, J.W. Chew, M. Fujiwara, and R.D. Braatz. Comparative performance of concentration and temperature controlled batch crystallizations. *Journal of Process Control*, 18(3-4):399–407, 2008.
- [16] A.D. Randolph and M.A. Larson. *Theory of particulate processes*. Academic Press San Diego, CA, 1971.

- [17] L. Rozsa. Seedmaster 2: A universal crystallization transmitter and automatic seeding device. *International Sugar Journal*, 1296:683, 2006.
- [18] N. Sanzida and Z.K. Nagy. Iterative learning control for the systematic design of supersaturation controlled batch cooling crystallisation processes. *Computers & Chemical Engineering*, 59:111–121, 2013.
- [19] T. Soderstrom. Errors-in-variables methods in system identification. *Automatica*, 43(6):939–958, 2007.
- [20] A. Van den Bos. *Parameter estimation for scientists and engineers*. Wiley-Interscience, 2007.
- [21] J. Vissers, M. Forgione, S.S. Kadam, P.J. Daudey, T. Backx, A.E.M. Huesman, H.J.M. Kramer, and P.M.J. Van den Hof. Novel control of supersaturation on an industrial scale pharmaceutical batch crystallizer. In *Proceedings of the 18th International Symposium on Industrial Crystallization*, pages 141–142, 2012.
- [22] M. Volckaert, M. Diehl, and M. Swevers. A two step optimization based iterative learning control algorithm. In *Proceedings of the Dynamic Systems and Control Conference*, pages 579–581, Cambridge, Massachusetts, USA, September 2010.
- [23] W. Xie, S. Rohani, and A. Phoenix. Extended kalman filter based non-linear geometric control of a seeded batch cooling crystallizer. *The Canadian Journal of Chemical Engineering*, 80(1):167–172, 2002.
- [24] J. Zhang, J. Nguyen, Z. Xiong, and J. Morris. Iterative learning control of a crystallisation process using batch wise updated linearised models. In *Proceedings of the 2009 Chinese Control and Decision Conference.*, pages 1734–1739. IEEE, 2009.